

Effect of Acid Treatment on the Functionalization of Surface, Structural and Textural Properties of Carbon Nanotubes Taunit

Z.R. Ismagilov*, S.A. Yashnik, N.V. Shikina, E.V. Matus, O.S. Efimova,
A.N. Popova, A.P. Nikitin

Federal Research Center of Coal and Coal Chemistry, Institute of Coal Chemistry and Material Science SB RAS,
18 Sovetskij pr., Kemerovo, 650000, Russia

Article info

Received:
15 March 2019

Received in revised form:
28 April 2019

Accepted:
15 June 2019

Keywords

Carbon nanotubes
Surface oxidation
Oxygen-bearing groups
Raman spectroscopy
FTIR spectroscopy

Abstract

The role of acid treatment of Taunit carbon nanotubes in the formation of oxygen-containing functional groups on its surface as well as morphological and textural properties was studied. Acid treatment was carried out in an HNO₃ solution or its mixture with H₂SO₄ under mild conditions (85 °C/1 h) with subsequent washing with distilled water or without washing. Properties of the initial and oxidized samples were investigated using elemental carbon, hydrogen, nitrogen, oxygen (CHNO) analysis, BET (Brunauer-Emmett-Teller) determination of surface area, X-ray diffraction, Raman and Fourier Transform Infrared Spectroscopy (FTIR) spectroscopy, and hydrogen temperature-programmed reduction. Treatment with HNO₃ and HNO₃/H₂SO₄ mixture was shown to be efficient for the formation of various oxygen-containing groups on the Taunit surface; therewith, the water washing step also contributed to functionalization of the surface. Depending on the oxidant, acid treatment increased graphite and oxygen content in the samples by a factor of 3–4.5. Treatment with HNO₃ without water washing exerted a weak effect on the graphite structure ordering, the concentration of aliphatic groups was high as compared to other oxidation conditions. Treatment of Taunit with the HNO₃/H₂SO₄ mixture, on the contrary, increased the number of defects in graphite layers and decreased the concentration of aliphatic structures.

1. Introduction

Carbon materials are widely used as catalyst supports, adsorbents, electrodes for supercapacitors, reinforcing fillers of polymers, fuel cell electrodes, biosensors, for the delivery of therapeutic preparations in cells, etc. [1–4]. Such a wide application of carbon materials is based on the variety of their morphological structures (nanotubes, nanofibers, amorphous carbon, and others), electronic properties, chemical stability in aggressive media, inertness toward the supported catalytically active component, the possibility of recovering the deposited noble metals by burning of the support, etc.

Graphitic nanotubes and nanofibers are obtained by decomposition (pyrolysis) of carbon-containing gases over metal catalysts [5–9]. The unique mechanical, electronic and thermal properties of nanotubes and nanofibers are provided by specific conditions of their synthesis. Carbon nanotubes (CNTs) consist of coaxial carbon layers, the number of which varies from 1 to 50, and have a cavity inside the tube [10]. Carbon nanofibers (CNFs) have the herringbone or platelet structure, which is determined by the arrangement of graphene layers relative to the fiber growth axis [11–14]. In CNFs, in distinction to carbon nanotubes, multiple cuts or partially closed edges of graphenes terminate at the external surface of the fiber, which makes it possible to use CNFs in catalysis. The CNT surface can readily be functionalized, thus opening a way for selective deposition of active metals [15].

*Corresponding author. E-mail: zinfer1@mail.ru

Nevertheless, the application of CNTs and CNFs for the synthesis of supported catalysts is limited by surface hydrophobicity of these materials and their low ability to homogeneous dispersion in many solvents. In addition, the high nonpolar surface of such materials results in the formation of the catalyst active components that are weakly bound to the surface, for example, noble metals. This may lead to the removal of active metals from CNT and CNF surface and fast deactivation of the catalysts in liquid-phase processes. This problem can be minimized by the surface modification of carbon nanomaterials with oxygen-containing functional groups [16–20], such as carboxy, carboxy anhydride, lactone, phenol, carbonyl, quinone, xanthene or ether groups. Several methods are employed to functionalize carbon material surface with oxygen-containing groups [21]. For example, methods of wet etching of carbon nanomaterials in concentrated solutions of acids – HNO_3 [16, 22, 23] and $\text{HNO}_3/\text{H}_2\text{SO}_4$ mixtures [16–18] were carefully elaborated. Ros et al. [16] estimated the efficiency of different compounds (HNO_3 , mixtures of HNO_3 and H_2SO_4 , KMnO_4 , H_2O_2) in wet etching of CNF surface and concluded that the mixture of concentrated nitric and sulfuric acids is most efficient for the formation of oxygen-containing groups on defect surface sites and, which is essential, does not produce changes in the graphite structure of CNFs. Darmstadt et al. [24] demonstrated that boiling in nitric acid not only oxidizes the surface but also decreases the ordering of the CNF graphitic structure. In multiwalled CNTs (MCNTs) with a low density of defects on the lateral walls, acid treatment provides the selective formation of $-\text{COOH}$ and $-\text{OH}$ groups at the ends of nanotubes, where many reactive and defect sites are located. Such selective action of acids is important, for example, for specific functionalization of nanotubes by oligonucleotides [25]. In addition to wet etching, methods of plasma [19, 26], photochemical [27] and electrochemical oxidation of carbon materials are also employed [20]. Thermal treatment in an inert atmosphere is conventionally employed, on the contrary, to remove oxygen groups and defects in order to increase ordering of the CNF graphite structure. Nevertheless, thermal treatment at relatively high temperatures in an oxygen-containing atmosphere facilitates the burnout of amorphous carbon and oxidation of the surface of a graphite-like carbon material. Thus, in [28], heating of MCNTs in the air to $400\text{ }^\circ\text{C}$ was used to enhance hydrophilicity by generating surface oxygen-containing groups and defects on nanotube walls.

Thus, wet acid activation of carbon materials is a well-elaborated method now. However, characterization of activated carbon materials was performed mostly using the laboratory CNT samples, whereas the commercial CNT samples were investigated only in a few works, which gave contradictory results. There are some studies where the gas-phase oxidation of commercial Taunit CNTs was performed in nitric acid [29] and H_2O_2 vapor [30]. The oxidation by HNO_3 vapor was efficient at $140\text{ }^\circ\text{C}$, which is the temperature at which a high concentration of carboxy groups on the surface was reached. However, the uniformity of carboxy groups distribution on the Taunit surface depended on the chemical composition of CNTs and instrumentation of the process. When CNTs were oxidized in a 37% aqueous solution of H_2O_2 , the degree of surface functionalization by $-\text{OH}$ and $-\text{COOH}$ groups was quite low even at temperatures above $140\text{ }^\circ\text{C}$, although their concentration tended to increase with temperature elevation. Wet treatment in concentrated nitric acid at $100\text{ }^\circ\text{C}$ seems to be unsuitable for functionalization of Taunit because the destruction of its surface layers was observed already after the treatment for 2 h [31].

In recent years, there appeared several studies exploring the possibility to apply carbon nanomaterials and the related catalysts for oxidative desulfurization (ODS) of fuels [32], particularly for the selective liquid-phase oxidation of sulfur compounds of thiophene and dibenzothiophene series to corresponding sulfoxides and sulfones. In refs. [33–36], supported catalysts based on activated carbon were studied in the liquid-phase oxidation of sulfur; it was shown that percarboxylic acid groups, which are formed in the reaction on defects of basal planes of the carbon lattice, accelerate the reaction [37]. A study of oxidized graphene and CNTs revealed the effect of the surface chemical composition and graphitization degree on the catalytic activity of carbon material in the oxidation of dibenzothiophene [38]. Carbon nanotubes with high graphitization degree demonstrated high catalytic activity in the oxidation of dibenzothiophene owing to their high electronic conduction [38], which provided electron transfer in the redox reaction. On the other hand, in [39] it was supposed that carbonyl groups and surface defects play an important role in the ODS process. In [38], structural, textural and surface properties of carbon nanotubes, for example, the Taunit CNTs, were shown to be essential for ODS. The ODS process requires the minimum differences in thermal stability of initial and oxidized CNTs.

The goal of this work was a detailed investigation of the composition of functional groups as well as the morphology, textural and structural features of Taunit carbon nanotubes, which are formed upon wet acid activation in HNO_3 and $\text{HNO}_3/\text{H}_2\text{SO}_4$. Treatment with acids was carried out under mild conditions: temperature 85 °C and treatment time 1 h; this was made to preserve the mechanical properties of CNTs and prevent the destruction of surface layers, which was earlier revealed for Taunit [31].

2. Materials and methods

2.1. Materials

Taunit carbon nanotubes (NanoTechCenter Ltd., Tambov, Russia) are represented by quasi-one-dimensional nanostructured filamentary graphite polycrystals, mostly of cylindrical shape with the internal channel. The initial CNT sample was dried at 170 °C in Ar for 2 h. The sample was denoted as **T1**.

2.2. Oxidation of CNTs

The oxidation of CNTs was performed using concentrated HNO_3 acid or an $\text{HNO}_3/\text{H}_2\text{SO}_4$ mixture at a volume ratio 1/1. A CNT sample was moistened with distilled water and poured with a specified amount of acid. A ratio of the CNT weight to the volume of liquid was 1/10. The temperature was raised to 85 °C and the sample was held at this temperature for an hour under constant stirring. After cooling to room temperature, the CNT suspension was diluted fivefold with distilled water and filtered on a vacuum Teflon filter. The sediment was then washed off repeatedly with hot water ($\text{H}_2\text{O}/\text{CNT} = 50/1$) to obtain the neutral reaction of wash water. After the oxidation procedure, the samples were dried under a lamp and then at 120 °C for 10 h. The samples treated with HNO_3 and $\text{HNO}_3/\text{H}_2\text{SO}_4$ were denoted as **T1N_{wash}** and **T1NS_{wash}**, respectively.

To reveal the effect of washing, one of the CNT samples treated with concentrated nitric acid at 85 °C was dried at the same temperature without water washing. The sample was denoted as **T1N**.

2.3. Investigation of physicochemical properties

The content of carbon, hydrogen, nitrogen, sulfur and oxygen was measured on a Thermo Flash

2000 (Thermo Scientific, USA) analyzer by burning the sample in reactors filled with CuO/Cu (for C, H, N, S detection) and nickel-plated carbon with quartz filings (for O detection) at a temperature of 1000 °C. The content of the elements was calculated by averaging the values of three parallel measurements.

X-ray diffraction (XRD) analysis was carried out on a Bruker D8 ADVANCE A25 powder X-ray diffractometer ($\text{CuK}\alpha$ radiation, Ni filter on the secondary radiation-beam) at room temperature by polycrystal method. The diffraction patterns were recorded at great accumulation times (up to 1.5 s) and a scanning step of 0.02°. ICDD and PDF2 databases were used for phase identification from diffraction peaks.

Raman spectra were recorded on a Renishaw Invia Raman Microscope spectrometer with the argon laser as an excitation source ($\lambda = 514.5$ nm), diffraction lattice 1800 pieces/mm, and a $\times 50$ long-focus objective able to focus a laser spot with the diameter up to 2 μm on a plane-parallel surface.

Textural properties of the samples were examined by the low-temperature nitrogen adsorption using an ASAP-2020 Micromeritics volumetric vacuum static setup. Specific surface area (S_{BET} , m^2/g) of the samples was obtained by the analysis of N_2 adsorption-desorption isotherms taken at -196 °C (77 K). Prior to adsorption measurements, the samples were dried in a drying oven at 105 ± 5 °C to a constant weight and then evacuated directly in a special port of the setup at 200 °C for 12 h to a residual pressure not higher than 0.65 Pa. The nitrogen adsorption-desorption isotherms were measured in the region of equilibrium relative vapor pressures from 10^{-3} to 0.995 P/P_0 . The specific surface area of the pores was calculated by the Brunauer-Emmett-Teller (BET) method. The micropore and mesopore volume was determined using the comparative t-Plot method and the Barrett-Joyner-Halenda (BJH) method, respectively. The average pore diameter was estimated by the formula $D_{av} = 4V_{ads}/S_{\text{BET}}$. The measurement error was 5%.

FTIR spectra were recorded on an Infracum FT-08 (Lumex, St.-Petersburg) Fourier transform IR spectrometer in a mixture with KBr at a weight ratio 1:130. A mixture of CNT with KBr was stirred in a vibromill for 3 min to obtain a homogeneous substance. After that, the mixture was pressed in a pellet at a pressure of 20 MPa. FTIR spectra were recorded in a range of 350–3000 cm^{-1} using 256 scans.

Sample stability to reduction was studied using temperature-programmed reduction with hydrogen (H_2 -TPR) on a setup equipped with a flow reactor and a heat conductivity detector. A Test-1 analyzer was used to identify gases (CH_4 , CO , and others), which were formed during H_2 -TPR experiment. The reduction was carried out in the temperature range from 25 to 900 °C with a ramp rate 10 °C/min; a mixture of 10% H_2 in Ar was passed through the sample at a rate of 30 cm^3 /min. Before the experiment, the sample was treated in Ar blown through the reactor with a rate of 30 cm^3 /min at 300 °C for 30 min. The weight of the sample was 50 mg, and the size of the particles, 250–500 μm . To prevent exothermic effects, the sample was mixed with 50 mg of quartz having the same particle size. Water formed during the reduction was removed from the gas mixture by freezing in a trap at –70 °C. The amount of consumed hydrogen was calibrated with respect to hydrogen consumed for the reduction of copper oxide under similar conditions, assuming that CuO is completely reduced in a single step.

3. Results and discussion

Figure 1 displays SEM images of unoxidized Taunit CNT sample. Its microstructure is represented by nanotubes with the external diameter 20–50 nm and length greater than 2 μm (the images were afforded by the manufacturer – <http://www.nanotc.ru/productions/87-cnm-taunit>). The arrowed bright white spots on the images are the Ni-Fe particles, which serve as the catalyst of CNT growth. The tube walls are perfectly smooth and virtually free of structural defects.

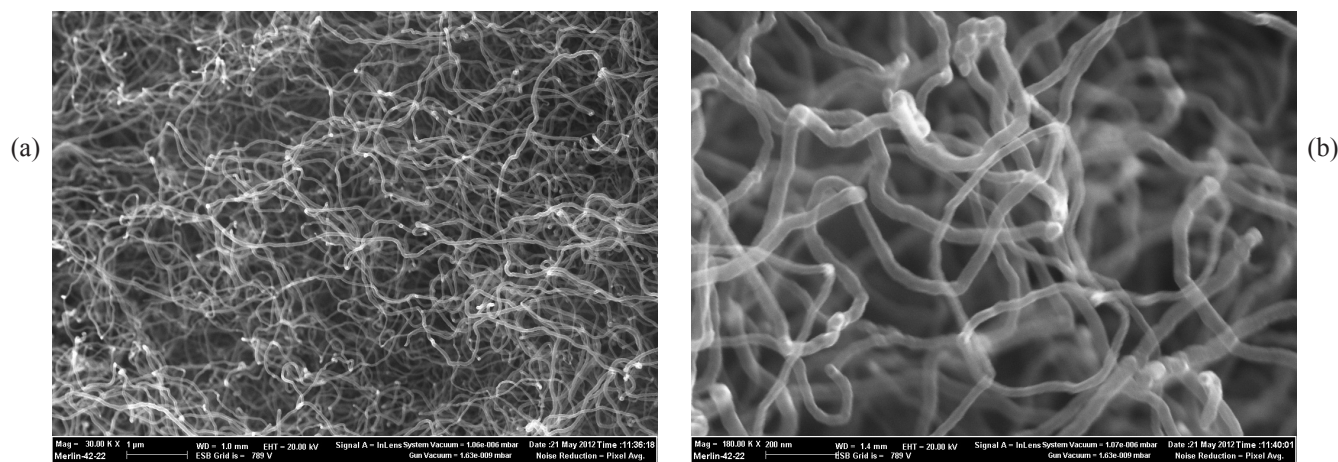


Fig. 1. SEM images of Taunit carbon nanotubes at different magnification: (a) – the label corresponds to 1 μm , (b) – 200 nm.

3.1. Chemical composition of CNTs

Investigation of the composition of CNT samples by CHNSO analysis (Table 1) before oxidation (T1) and after the oxidation with acids (T1N, T1N_{wash}, T1NS_{wash}) revealed that acid treatment of the carbon material increases the content of carbon and decreases the content of hydrogen, which is accompanied by a decrease in the $[H]/[C]$ ratio. The indicated changes in the composition of carbon material testify to an increase in its graphitization degree. Graphitization of CNTs may increase due to dissolution of the amorphous part of carbon in acids. Oxygen content in the oxidized samples depends on the treatment conditions. The initial sample T1 may contain a certain amount of oxygen in the surface oxygen-containing groups, which are stable in Ar at temperatures up to 170 °C. Treatment of the T1 sample in HNO_3 (T1N and T1N_{wash}) increased oxygen content by a factor of 3, whereas its treatment in the HNO_3/H_2SO_4 mixture (T1NS_{wash}) – by a factor of 4.5. According to the chemical analysis data on oxygen, the concentration of oxygen-containing groups in the oxidized CNT samples increases in the series: T1N_{wash} < T1N < T1NS_{wash}.

3.2. Ordering of the CNT structure according to XRD and Raman spectroscopy data

The diffraction pattern of the initial and oxidized CNT samples (Fig. 2) contains peaks of graphitic carbon, nickel-iron metallic alloy with the FCC lattice (2θ : ~44, 52, 76, 93, and 98°), and magnesium oxide phase (2θ : ~ 37, 43, 63, 75, 79, and 94°). Ni-Fe and MgO entered the catalyst composition,

Table 1
Elemental analysis of CNT samples of the Taunit series before and after oxidation

#	Sample	C, %	H, %	[H]/[C]	N, %	S, %	O, %
1	T1	91.72	0.35	0.046	0	0	0.78
2	T1N	93.07	0.30	0.039	0.15	0	2.84
3	T1N _{wash}	93.04	0.31	0.040	0.21	0	2.49
4	T1NS _{wash}	92.11	0.33	0.043	0.19	0	3.52

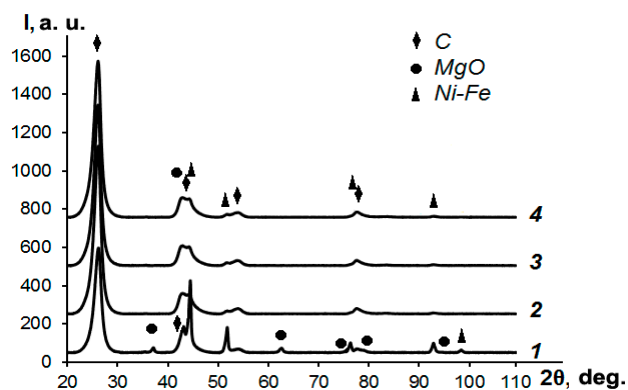


Fig. 2. The diffraction patterns of Taunit CNTs: 1 – unoxidized sample T1; oxidized samples: 2 – T1N, 3 – T1N_{wash}, and 4 – T1NS_{wash}.

and a part of them remained in T1. There are some differences between diffraction patterns of the initial and oxidized samples. A slight broadening of the graphite phase peak ($2\theta = 26^\circ$) and an increase in its intensity for the samples treated with acids are observed. Broadening of the graphite line may indicate a decrease in the crystallite size of graphite after the oxidation of CNTs, whereas an increase in intensity of the graphite line for the oxidized samples testifies to a growth of the graphite component in the samples due to dissolution of amorphous carbon in acids. This is consistent with the chemical analysis data. The position of graphite peaks does not change in the process. The intensity of the peaks corresponding to the mineral phase, MgO and Ni-Fe alloy considerably decreases for all the oxidized samples. Most likely, treatment with acids leads to the dissolution of weakly condensed carbon and partial removal of the CNT growth catalyst from the cavities of nanotubes. In 1994, Tsang et al. [40] investigated carbon nanotubes that were treated with concentrated HNO_3 at 140°C for 4.5 and 24 h; the HRTEM study showed that treatment with the acid opens the nanotube edges. The fraction of open nanotubes, which were free of the catalyst particles, reached 80–90% depending on the

time of the experiment [40]. A similar conclusion was made in [16, 18], where XRD study of carbon nanofibers revealed a decrease in the concentration of mineral phase in the samples after treatment with acids. Thus, dissolution of the growth catalyst during treatment of carbon nanomaterials in mineral acids is a general trend leading to the catalyst removal from the carbon nanomaterial with different arrangement of graphene layers.

In our experiments, peaks corresponding to the Ni-Fe phase were not observed for the oxidized samples; only peaks of the MgO phase, the amount of which is very low as compared to unoxidized sample T1, were identified. It seems interesting that in the T1N sample, which was oxidized by HNO_3 but not washed with water, the amount of such phases is comparable with that in the washed samples T1N_{wash} and T1NS_{wash}, from which the dissolved Ni, Fe and Mg compounds were removed by washing with water. In the case of T1N sample, such compounds may become X-ray amorphous after CNT drying and cannot be identified by XRD.

Raman spectroscopy is the most informative method for studying the structural disorder and defectness of graphite-like materials. It is known [24, 41] that the Raman spectrum of crystalline graphite is characterized only by G band in the wavenumber region near 1575 cm^{-1} . In the spectra of defect structures of polycrystalline graphite and other carbonized materials, bands appear in the region of 1355 cm^{-1} (D band) and in some cases at 1620 cm^{-1} (D' band or the so-called “peak of defects”) [24]. The appearance of D band is observed in the case of symmetry breakdown of the atoms that are close to the ends of graphite layers, when the forbidden vibration of the A_{1g} type becomes possible [41]. D' band is due to modifications in the hexagonal ring tension caused by the arrangement of the electronic cloud. This band is typical of the graphite-like materials with many defects and weakens with an increase in their structural ordering [19]. The ratio of the areas of D and G bands (I_D/I_G)

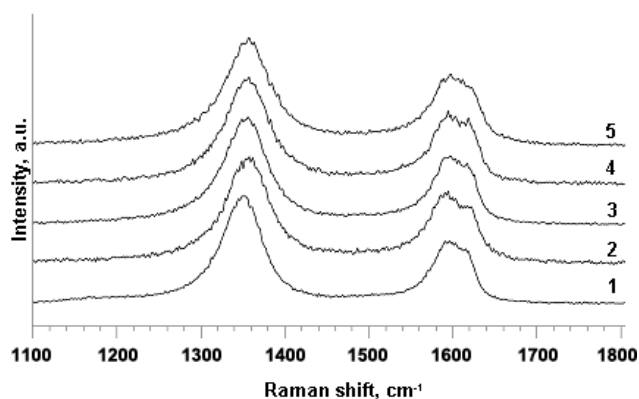


Fig. 3 Raman spectra of Taunit CNTs: 1 – unoxidized sample T1; oxidized samples: 2 – T1N, 3 – T1N_{wash}, 4 – T1NS_{wash} dark phase, and 5 – T1NS_{wash} bright phase.

is commonly used for estimating the disorder of graphite-like systems. Another control measure of the structural ordering is the ratio of D band overtone (2D band) to G band: the greater is the ratio, the higher is the graphitization degree; however, this trend holds true for extended structures, to which CNFs cannot be attributed.

Figure 3 displays Raman spectra of the Taunit CNT samples before and after acid treatments. Raman spectra of all the samples contain two main peaks D and G in the region of 1350 and 1590 cm⁻¹, respectively. A shoulder near 1620 cm⁻¹ testifies to the presence of D' band. Raman spectra of the tested samples, including the initial unoxidized T1 sample, differ from the Raman spectra of single- and double-walled CNTs (SWCNTs and DWCNTs, respectively) reported in the literature [42] by a higher intensity of D band as compared to G band, which indicates a great number of structural defects in Taunit. On the other hand, in the Raman spectra of multiwalled CNT samples [42], D line had a higher intensity than G line, similar to the case of Taunit samples. Data on the processed Raman spectra of Taunit samples are listed in Table 2.

According to Table 2, an increase in the D band half-width is observed for all the oxidized samples, and broadening of G band in comparison with unoxidized T1 sample is observed for the majority of samples; this may testify to a decrease in the size of carbon crystallites. This assumption is confirmed by XRD data, which revealed broadening of graphite lines after the oxidation of CNTs. Differences in structural ordering of the carbon framework between T1 and T1N are insignificant: $I_D/I_G(T1N) = 1.99$ and 1.97 , respectively. Disordering of T1N_{wash} and T1NS_{wash} samples is somewhat higher: $I_D/I_G(T1N_{wash}) = 2.10$ and 2.29 . The growth of defectness may be caused by the disturbance of graphene layers symmetry during the formation of functional groups [31]. Table 2 lists values of Raman parameters for the T1NS_{wash} sample, which were obtained in different regions of the sample because examination of the sample on an optical microscope revealed dark and bright surface regions (Fig. 4). Differences were found in the Raman spectra obtained for these regions; hence, the microstructure of the CNT sample treated with the HNO₃/H₂SO₄ mixture is inhomogeneous. The concentration of defects is higher in the bright part of the sample.

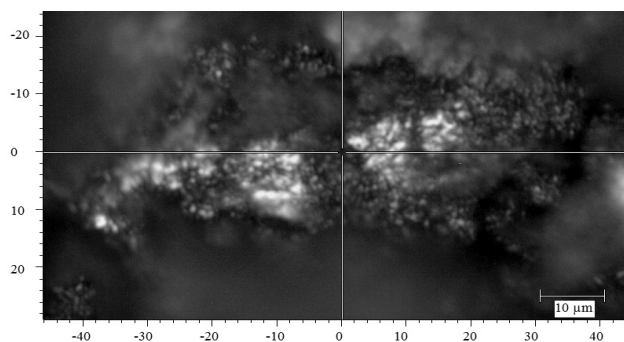


Fig. 4. A photo of T1NS_{wash} sample obtained on an optical microscope at a $\times 50$ magnification.

Table 2
Position, half-width of D and G bands, and I_D/I_G ratio for all CNT samples

Sample	D band		G band		I_D/I_G
	Position, cm ⁻¹	Half-width, cm ⁻¹	Position, cm ⁻¹	Half-width, cm ⁻¹	
T1	1349	57	1592	45	1.99
T1N	1356	62	1588	52	1.97
T1N _{wash}	1353	63	1590	46	2.10
T1NS _{wash} dark	1355	65	1588	41	2.29
T1NS _{wash} light	1356	66	1593	60	2.10

According to the data obtained, the greatest amount of defects is observed in T1N_{wash} and T1NS_{wash} samples. They have the highest I_D/I_G values. These data are consistent with the results of other studies, which demonstrated a decrease in the graphite ordering after the oxidation of carbon materials with graphitic structure [25, 30]. Overall, the I_D/I_G ratio slightly changes after acid treatment. A possible reason is that the acids weakly interact with the defects of nanotubes in their conglomerates [43].

3.3. Textural properties of CNTs

The obtained textural characteristics, namely, the values of specific surface area (S_{BET} , m²/g), pore volume (the total pore volume V_{Σ} , cm³/g; the micro- and mesopore volumes V_{micro} and V_{meso} , cm³/g) and average pore diameter (D_{pores} , Å) of the tested samples, are listed in Table 3. All the samples have close textural parameters (specific surface area and pore volume) before and after the oxidation. A minor increase in specific surface area (by 10% on the average) after treatment with acids is provided by an increment in the micropore volume, which is related to etching of the surface of CNT walls with acids; an increase in the pore volume is provided by the removal of metal catalyst particles and opening of the internal channels of nanotubes.

The shape of nitrogen adsorption-desorption isotherms (Fig. 5a) testifies to the mixed type of the pore structure consisting of meso- and micropores. The pore size distribution (Fig. 5b) indicates the polymodal nature of the pore structure with a wide set of pore sizes from 20 to 1000 Å. The effective pore diameter corresponds to the pores with the size of 40 Å. The oxidative treatment of CNTs with acids exerts virtually no effect on the pore size distribution. Treatment of nanotubes with the HNO₃/H₂SO₄ mixture promotes the formation of a greater amount of small pores with the diameter 20–35 Å; accordingly, the smallest average pore diameter and the greatest specific surface area are

Table 3
Textural properties of CNT samples
of the Taunit series before and after oxidation

Sample	S_{BET} , m ² /g	V_{Σ} , cm ³ /g	V_{micro} , cm ³ /g	V_{meso} , cm ³ /g	D_{pores} , Å
T1	180	0.32	0.009	0.30	71
T1N	190	0.34	0.014	0.32	71
T1N _{wash}	197	0.36	0.015	0.33	72
T1NS _{wash}	196	0.33	0.013	0.31	68

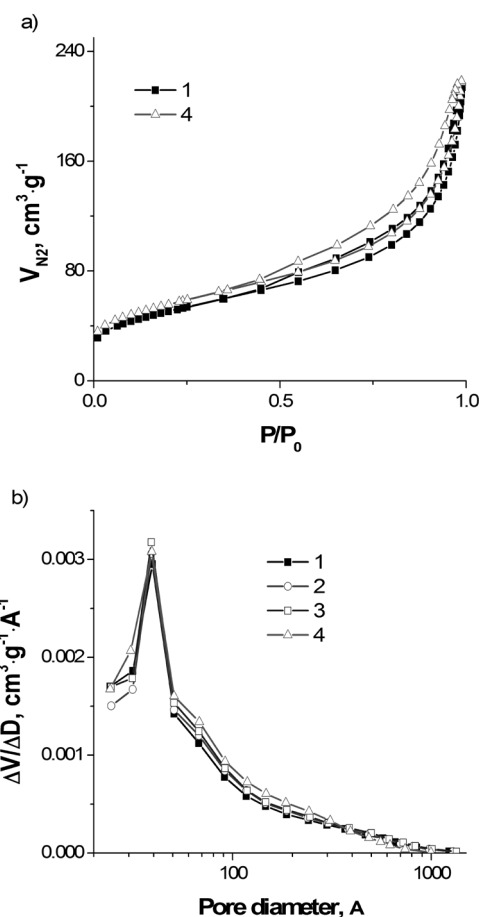


Fig. 5. Nitrogen adsorption-desorption isotherms (a) and differential pore size distribution (b) in Taunit CNT samples before and after the oxidation. 1 – unoxidized sample T1; oxidized samples: 2 – T1N, 3 – T1N_{wash}, and 4 – T1NS_{wash}.

observed for the T1NS_{wash} sample. Minor changes in the pore structure parameters of CNTs after the oxidation testify that acid treatment affects mostly the surface properties, whereas the bulk properties remain unchanged.

3.4. State of the surface and bulk groups in CNTs according to FTIR spectroscopy

FTIR spectra of the initial and oxidized CNT samples (Fig. 6) are characterized by a wide set of absorption bands (a.b.) in the region of 500–3000 cm⁻¹; some of them are caused by vibrations of the lattice and functional groups of the carbon material, while another part of a.b. (in the region of 670–520 cm⁻¹) – by components (MgO, NiO) of the CNT growth catalyst. In addition, the spectra contain a.b. in the region of 1630–1642 cm⁻¹, which is attributed to deformation vibrations of water [44]. Let us discuss some general and specific regularities in FTIR spectra of the initial and oxidized CNT samples.

First, the spectra of unoxidized sample T1 and acid-activated samples T1N, T1N_{wash} and T1NS_{wash} contain broad bands in the region of 875–880 and 1572–1582 cm⁻¹, which were assigned in [45] to vibrational modes A_{2u} and E_{1u} in the crystal structures of graphite. In addition, the spectra contain a broad band in the region of 1200–1210 cm⁻¹, which corresponds to vibrations of the defect graphitic structure with distorted translational symmetry [45]. The maximum of the indicated band shifts from 1178 to 1200–1207 cm⁻¹ for the oxidized samples T1N, T1N_{wash} and T1NS_{wash} (Fig. 6).

Second, bands with the maxima at 2954, 2895 and 2834 cm⁻¹ are observed in the spectrum of the initial sample T1. The first two bands correspond to asymmetric (ν₁) and symmetric (ν₂) stretching vibrations of CH₃ groups, whereas the 2834 cm⁻¹ band – to symmetric (ν₂) stretching vibrations of CH₂ group [44]. Note that the band of asymmetric stretching vibrations of CH₂ groups (commonly at 2950–2925 cm⁻¹) may be masked by a broad a.b. at 2925–2850 cm⁻¹. Deformation vibrations (δ) of the C-H bond in CH₂/CH₃ groups (commonly at 1370–1450 cm⁻¹ [44]) show up in the spectrum of the sample as the band at 1425 cm⁻¹. Therewith, spectra of the oxidized samples T1N_{wash} and T1NS_{wash} contain bands at 2920, 2849 and 1380 cm⁻¹ corresponding to CH₂ groups. In addition, the T1N spectrum has a shoulder in the region of 2955 cm⁻¹ indicating the presence of CH₃ groups, although their amount is smaller as compared to sample T1. The band intensity of CH₂/CH₃ stretching vibrations at 2919 and 2849 cm⁻¹ decreases in the spectra of T1N_{wash} and T1NS_{wash} samples. T.G. Ros et al. [16, 46] in their study of carbon nanofibers with a different arrangement of graphite layers concluded that the band assigned to CH₂/CH₃ stretches appears on

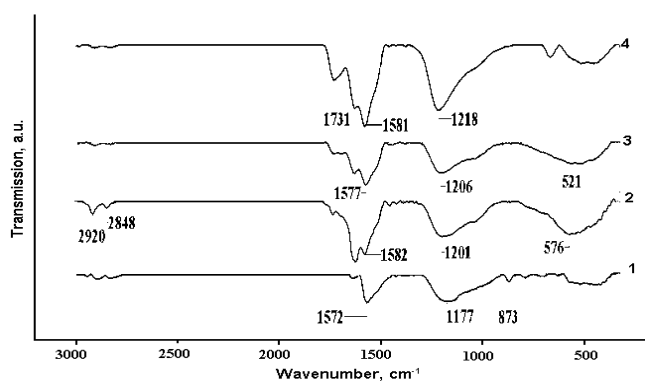


Fig. 6. FTIR spectra of Taunit CNTs: 1 – unoxidized sample T1; oxidized samples: 2 – T1N, 3 – T1N_{wash}, and 4 – T1NS_{wash}.

the graphite structure defects. The intensity of this band decreases after treatment in acids due to a partial transformation of C-H bonds to C-O upon formation of the oxygen-containing groups. H. Darmstadt et al. [24] made a similar conclusion from the analysis of surface enhanced Raman (SER) spectra of carbon materials; they supposed that a decrease in the concentration of aliphatic structures after oxidative surface treatment is caused by their oxidation or decomposition. In [24], a direct dependence between the concentration of aliphatic structures and disordering of graphite structures was revealed. It seems interesting that according to the I_D/I_G ratio of lines in the Raman spectra, the T1N sample is the most ordered among the studied ones, whereas the T1NS_{wash} sample has the highest content of structural defects and the minimum intensity of bands at 2910, 2839 and 1462 cm⁻¹. Therefore, similar to [24], we can suppose that the graphite structure ordering and the concentration of aliphatic structures are interrelated.

Third, the spectra of oxidized Taunit samples contain bands with the maxima at 1720–1740 and 1693 cm⁻¹, which are absent in the spectrum of the initial sample T1. Bands in the region of 1700–1740 and 1690–1655 cm⁻¹ can reliably be attributed to stretching vibrations of the C=O bond in carboxy (-COOH) and quinone groups [16, 44, 46, 47], respectively. In this case, bands in the region of 1440–1395 and 1205–1260 cm⁻¹ may be caused not only by deformation vibrations of CH₂/CH₃ groups and defects of graphitic structures, respectively, but also by a combination of deformation vibrations of C-O and C-H bonds in carboxy groups [44]. Note that monomeric -COOH groups, in distinction to the hydrogen-bound groups, have the band at 1190–1075 cm⁻¹ corresponding to C=O vibrations [44], which can be observed in our study as a shoulder near 1075 cm⁻¹ and indicates their presence in the composition of oxidized samples. In addition, the band at 1380 cm⁻¹ may correspond to vibrations of N=O in NO₂, for which the symmetric and asymmetric bands are in the region of 1370–1390 and 1550–1580 cm⁻¹, respectively. As shown by analysis of the spectra, the intensity ratio of 1720 and 1693 cm⁻¹ bands depended on the conditions of oxidative treatment of Taunit. The T1NS_{wash} sample had the maximum intensity of the indicated bands and they were not separated. The intensities of T1N and T1N_{wash} samples were much lower than that of T1NS_{wash}, but comparable with each other. The oxygen content estimated by CHNO analysis correlates with the intensity of a.b.

at 1720 and 1693 cm^{-1} ; the maximum oxygen content is observed for $\text{T1NS}_{\text{wash}}$, while in T1N and T1N_{wash} it is lower by 19 and 30%, respectively. Thus, the content of carboxy groups in the oxidized samples correlates with the I_D/I_G ratio in the Raman spectrum.

3.5. Stability of functional groups on the CNT surface estimated by H_2 -TPR

H_2 -TPR was used to investigate the stability of functional groups of the initial and oxidized CNT samples in reducing media.

H_2 -TPR profiles for the initial and oxidized CNT samples are displayed in Fig. 7. Profiles of all the samples contain two intense hydrogen adsorption peaks in the temperature region of 390–400 and 590–660 °C as well as the peak in the low-temperature region with the maximum at 195 °C, which has a very low intensity. The analysis of H_2 -TPR profiles shows that the amount of hydrogen adsorbed in separate temperature regions did not correlate with their oxygen content estimated by CHNO analysis. In the temperature region of 195 and 590–660 °C, the amount of adsorbed hydrogen reached a maximum for the initial sample T1, whereas in the region of 390–400 °C its minimum amount was observed. Therewith, the T1 sample contained 0.78 wt.% of oxygen, which is lower as compared to all the oxidized samples. The direct analysis of the gas mixture composition (using a Test-1 gas analyzer) at the TPR reactor outlet revealed that hydrogen is actually adsorbed in two quite wide temperature regions with the maxima near 400 and 635 °C. The medium temperature region of hydrogen adsorption 380–400 °C correlated with CO release, which was typical of both the initial and oxidized Taunit samples. Its amount was comparable for all the oxidized samples at 380–450 °C; however, for T1N and T1N_{wash} samples the CO release region was somewhat broader: 450 – 530 °C, where CO was not already released from the $\text{T1NS}_{\text{wash}}$ sample. For T1 and T1N samples, the high-temperature peak of hydrogen adsorption was accompanied by a release of methane and CO, which reached a maximum at 650 and 680 °C, respectively, whereas from T1N_{wash} and $\text{T1NS}_{\text{wash}}$ samples only CO was released. It should be noted that the CO amount released in the high-temperature region was comparable for T1N and T1N_{wash} samples, while for the $\text{T1NS}_{\text{wash}}$ sample it was lower by an order of magnitude. Unfortunately, the formation of CO_2 could not be

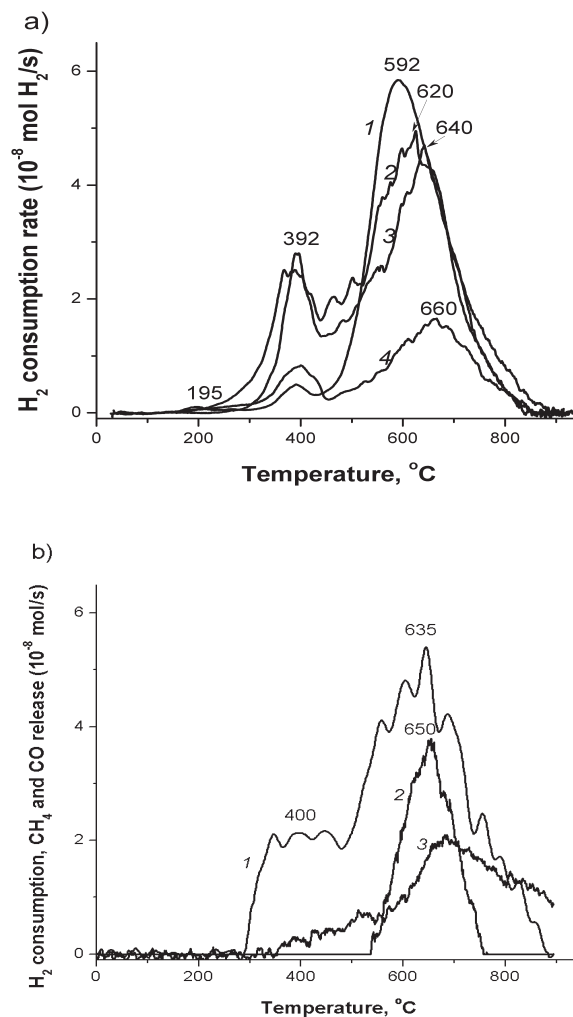


Fig. 7. a) H_2 -TPR profiles of the samples: 1 – unoxidized T1; oxidized samples: 2 – T1N , 3 – T1N_{wash} , and 4 – $\text{T1NS}_{\text{wash}}$. b) Concentration profiles of gases in H_2 -TPR experiment with the T1N sample. 1 – hydrogen consumption, 2 – methane release, and 3 – CO release.

detected by the gas analyzer because CO_2 (in the case of its formation) was frozen out together with water in a trap cooled to -70 °C before passing to the detector.

CO release in the medium temperature region testifies to the presence of carboxy groups in the oxidized samples; in the presence of hydrogen, these groups will selectively oxidize to phenol groups [48–50]. The reduction of carboxy groups ($-\text{COOH}$) to phenolic groups ($\text{C}-\text{OH}$) on the surface of CNTs oxidized by hydrogen peroxide was observed at 450–700 °C [49, 50]. Lactone groups and carboxy anhydride groups are reduced at temperatures above 430 °C with a release of CO and CO_2 [48], which may testify to their presence in T1N and T1N_{wash} samples, although CO_2 was not detected in this temperature region.

Methane can be formed during H₂-TPR of the initial Taunit sample due to the interaction of hydrogen with surface functional groups of CNTs [48] or with CO/CO₂, which appear upon decomposition of CNT functional groups [51]. This assumption is based on the known fact that selective methanation of CO and/or CO₂ catalyzed by metallic Ni particles [52, 53] proceeds in the hydrogen-containing medium, but commonly the reaction occurs at quite low temperatures (up to 200 °C [53]). But in this case, the ability to methanation of CNTs by hydrogen should depend on both the concentration of oxygen-containing groups in the sample and the content of metallic nickel. According to our experimental data, for Taunit samples, the amount of hydrogen and CH₄ adsorbed and released, respectively, in the high-temperature region of H₂-TPR experiment directly depended on the residual content of Ni-Fe in the CNT growth catalyst, but inversely depended on the oxygen content in the catalyst. In other words, the higher were the structural disordering (the I_D/I_G ratio) and the oxygen concentration (CHNO analysis and intensity of the band at 1720 cm⁻¹ in IR spectroscopy) and the lower was the Ni-Fe fraction, the higher was the stability of CNTs to methanation.

4. Conclusions

Carbon nanotubes Taunit were treated with concentrated acids, nitric acid and a mixture of nitric and sulfuric acids taken in the volume ratio 1/1 at a temperature of 85 °C for 1 h. According to CHNO analysis, the initial CNT sample not treated with acids already contains oxygen and hence the oxygen-containing groups. Acid treatment under mild conditions leads to the oxidation of the CNF surface and increases the oxygen content by a factor of 3–4. As shown by XRD studies, treatment with acids increases the content of graphite phase in the samples, which is related to the dissolution of weakly condensed carbon by acids. According to the Raman spectroscopy data, all CNT samples, including unoxidized and all oxidized samples, are characterized by a high I_D/I_G ratio, which indicates a high defectness of CNTs. Treatment with acids decreases the crystallite size of carbon and increases defectness of the graphite structure (if the procedure includes water washing after the oxidation step). The CNT sample oxidized by HNO₃ without water washing has the most ordered graphite structure in comparison with other oxidized samples. The use of the HNO₃/H₂SO₄ mixture produces

more pronounced changes in the graphite structure as compared to HNO₃. FTIR spectroscopy revealed that the use of HNO₃ without water washing and the HNO₃/H₂SO₄ mixture with subsequent washing provides the most efficient oxidation of the Taunit surface with the formation of various oxygen-containing groups. As shown by the BET method, treatment with acids virtually does not change the textural properties of CNTs. Thus, the oxidation of CNTs by acids changes mostly the surface properties and does not affect the bulk properties of CNTs.

Acknowledgment

This study was financially supported by the Russian Science Foundation (Project No. 19-13-00129). This study was accomplished using the research facilities of the Federal Research Center of Coal and Coal Chemistry of SB RAS.

The authors are grateful for the physicochemical investigations to Dudnikova Yu.N. and Malyshva V.Yu.

References

- [1]. X. Zhao, H. Chen, F. Kong, Y. Zhang, S. Wang, S. Liu, L.A. Lucia, P. Fatehi, H. Pang, *Chem. Eng. J.* 364 (2019) 226–243. DOI: [10.1016/j.cej.2019.01.159](https://doi.org/10.1016/j.cej.2019.01.159)
- [2]. M.T.H. Siddiqui, S. Nizamuddin, H.A. Baloch, N.M. Mubarak, M. Al-Ali, S.A. Mazari, A.W. Bhutto, R. Abro, M. Srinivasan, G. Griffin, *J. Environ. Chem. Eng.* 7 (2019) 1028122. DOI: [10.1016/j.jece.2018.102812](https://doi.org/10.1016/j.jece.2018.102812)
- [3]. F. Barroso-Bujans, R. Verdejo, M. Pérez-Cabero, S. Agouram, I. Rodríguez-Ramos, A. Guerrero-Ruiz, M.A. López-Manchado, *Eur. Polym. J.* 45 (2009) 1017–1023. DOI: [10.1016/j.eurpolymj.2008.12.029](https://doi.org/10.1016/j.eurpolymj.2008.12.029)
- [4]. A. Alonso-Lomillo, O. Rüdiger, A. Maroto-Valiente, M. Velez, I. Rodríguez-Ramos, F.J. Muñoz, V.M. Fernández, A.L. De Lacey, *Nano Lett.* 7 (2007) 1603–1608. DOI: [10.1021/nl070519u](https://doi.org/10.1021/nl070519u)
- [5]. L.B. Avdeeva, T.V. Reshetenko, Z.R. Ismagilov, V.A. Likhobolov, *Appl. Catal. A.* 228 (2002) 53–63. DOI: [10.1016/S0926-860X\(01\)00959-0](https://doi.org/10.1016/S0926-860X(01)00959-0)
- [6]. T.V. Reshetenko, L.B. Avdeeva, Z.R. Ismagilov, A.L. Chuvilin, V.A. Ushakov, *Appl. Catal. A.* 247 (2003) 51–63. DOI: [10.1016/S0926-860X\(03\)00080-2](https://doi.org/10.1016/S0926-860X(03)00080-2)
- [7]. O.Yu. Podyacheva, Z.R. Ismagilov, A.E. Shalagina, V.A. Ushakov, A.N. Shmakov, S.V. Tsybulya, V.V. Kriventsov, A.V. Ischenko, *Carbon* 48 (2010) 2792–2801. DOI: [10.1016/j.carbon.2010.04.008](https://doi.org/10.1016/j.carbon.2010.04.008)

- [8]. O.Yu. Podyacheva, A.N. Schmakov, Z.R. Ismagilov, *Carbon* 52 (2013) 486–492. DOI: [10.1016/j.carbon.2012.09.061](https://doi.org/10.1016/j.carbon.2012.09.061)
- [9]. V.V. Chesnokov, O.Y. Podyacheva, A.N. Shmakov, L.S. Kibis, A.I. Boronin, Z.R. Ismagilov, *Chinese J. Catal.* 37 (2016) 169–176. DOI: [10.1016/S1872-2067\(15\)60982-2](https://doi.org/10.1016/S1872-2067(15)60982-2)
- [10]. S. Iijima, *Nature* 354 (1991) 56–58. DOI: [10.1038/354056a0](https://doi.org/10.1038/354056a0)
- [11]. K.P. De Jong, J.W. Geus, *Catal. Rev.* 42 (2000) 481–510. DOI: [10.1081/CR-100101954](https://doi.org/10.1081/CR-100101954)
- [12]. P. Serp, M. Corrias, P. Kalck, *Appl. Catal. A Gen.* 253 (2003) 337–358. DOI: [10.1016/S0926-860X\(03\)00549-0](https://doi.org/10.1016/S0926-860X(03)00549-0)
- [13]. E. Antolini, *Appl. Catal. B Environ.* 88 (2009) 1–24. DOI: [10.1016/j.apcatb.2008.09.030](https://doi.org/10.1016/j.apcatb.2008.09.030)
- [14]. J.H. Bitter, *J. Mater. Chem.* 20 (2010) 7312–7321. DOI: [10.1039/C0JM00492H](https://doi.org/10.1039/C0JM00492H)
- [15]. J. Shariati, A. Haghtalab, A. Mosayebi, *J. Energy Chem.* 28 (2019) 9–22. DOI: [10.1016/j.jechem.2017.10.001](https://doi.org/10.1016/j.jechem.2017.10.001)
- [16]. T.G. Ros, A.J. van Dillen, J.W. Geus, D.C. Koningsberger, *Chem.–Eur. J.* 8 (2002) 1151–1162. DOI: [10.1002/1521-3765\(20020301\)8:5<1151::AID-CHEM1151>3.0.CO;2-%23](https://doi.org/10.1002/1521-3765(20020301)8:5<1151::AID-CHEM1151>3.0.CO;2-%23)
- [17]. J.H. Bitter, M.K. van der Lee, A.G.T. Slotboom, A.J. van Dillen, K.P. de Jong, *Catal. Lett.* 89 (2003) 139–142. DOI: [10.1023/A:1024744131630](https://doi.org/10.1023/A:1024744131630)
- [18]. M.L. Toebes, J.M.P. van Heeswijk, J.H. Bitter, A.J. van Dillen, K.P. de Jong, *Carbon* 42 (2004) 307–315. DOI: [10.1016/j.carbon.2003.10.036](https://doi.org/10.1016/j.carbon.2003.10.036)
- [19]. A.B. Dongil, B. Bachiller-Baeza, A. Guerrero-Ruiz, I. Rodríguez-Ramos, A. Martínez-Alonso, J.M.D. Tascón, *J. Colloid Interf. Sci.* 355 (2011) 179–189. DOI: [10.1016/j.jcis.2010.11.066](https://doi.org/10.1016/j.jcis.2010.11.066)
- [20]. C.M. Yoon, D. Long, S.M. Jang, W. Qiao, L. Ling, J. Miyawaki, C.K. Rhee, I. Mochida, S.H. Yoon, *Carbon* 49 (2011) 96–105. DOI: [10.1016/j.carbon.2010.08.047](https://doi.org/10.1016/j.carbon.2010.08.047)
- [21]. K.L. Klein, A.V. Melechko, T.E. McKnight, S.T. Retterer, P.D. Rack, J.D. Fowlkes, D.C. Joy, M.L. Simpson, *J. Appl. Phys.* 103 (2008) 061301. DOI: [10.1063/1.2840049](https://doi.org/10.1063/1.2840049)
- [22]. Y. Sato, K. Shibata, H. Kataoka, S. Ogino, F. Bunshi, A. Yokoyama, K. Tamura, T. Akasaka, M. Uo, K. Motomiya, B. Jeyadevan, R. Hatakeyama, F. Watari, K. Tohji, *Mol. Biosyst.* 1 (2005) 142–145. DOI: [10.1039/B501222H](https://doi.org/10.1039/B501222H)
- [23]. S. Lim, S.H. Yoon, I. Mochida, J.H. Chi, *J. Phys. Chem. B* 108 (2004) 1533–1536. DOI: [10.1021/jp036819r](https://doi.org/10.1021/jp036819r)
- [24]. H. Darmstadt, L. Summchen, J.-M. Ting, U. Roland, S. Kaliaguine, C. Roy, *Carbon* 35 (1997) 1581–1585. DOI: [10.1016/S0008-6223\(97\)00116-4](https://doi.org/10.1016/S0008-6223(97)00116-4)
- [25]. B.J. Taft, A.D. Lazareck, G.D. Withey, A.J. Yin, J.M. Xu, S.O. Kelley, *J. Am. Chem. Soc.* 126 (2004) 12750–12751. DOI: [10.1021/ja045543d](https://doi.org/10.1021/ja045543d)
- [26]. P.G. He, L.M. Dai, *Chem. Commun.* 3 (2004) 348–349. DOI: [10.1039/B313030B](https://doi.org/10.1039/B313030B)
- [27]. K.M. Metz, K.Y. Tse, S.E. Baker, E.C. Landis, R.J. Hamers, *Chem. Mater.* 18 (2006) 5398–5400. DOI: [10.1021/cm061563y](https://doi.org/10.1021/cm061563y)
- [28]. K. Wang, H.A. Fishman, H.J. Dai, J.S. Harris, *Nano Lett.* 6 (2006) 2043–2048. DOI: [10.1021/nl061241t](https://doi.org/10.1021/nl061241t)
- [29]. S.Yu. Gorski, T.P. Dyachkova, E.A. Burakova. *St. Petersburg Polytechnic University Journal of Engineering Science and Technology* [Nauchno-tehnicheskie vedomosti Sankt-Peterburgskogo gosudarstvennogo politehnicheskogo universiteta] 1 (2014) 108–112. (in Russian).
- [30]. T.P. Dyachkova, Yu.A. Khan, N.V. Orlova, S.V. Kondrashov, *Bulletin of Tambovsky State Technical University* [Vestnik Tambovskogo gosudarstvennogo tehnikeskogo universiteta] 22 (2016) 323–333 (in Russian). DOI: [10.17277/vestnik.2016.02.pp.323-333](https://doi.org/10.17277/vestnik.2016.02.pp.323-333)
- [31]. T.P. Dyachkova. *Phisiko-khimicheskie osnovy funktsializatsii I modifitsirovaniya uglerodnykh nanomaterialov*. Dokt. Diss. [Physico-chemical bases of functionalization and modification of carbon nanomaterials. Doct. Thes.]. Tambov, 2016. 404 p. (in Russian).
- [32]. Z. Ismagilov, S. Yashnik, M. Kerzhentsev, V. Parmon, A. Bourane, F.M. Al-Shahrani, A.A. Hajji, O.R. Koseoglu, *Catal. Rev.* 53 (2011) 199–255. DOI: [10.1080/01614940.2011.596426](https://doi.org/10.1080/01614940.2011.596426)
- [33]. G.X. Yu, S.X. Lu, H. Chen, Z.N. Zhu, *Carbon* 43 (2005) 2285–2294. DOI: [10.1016/j.carbon.2005.04.008](https://doi.org/10.1016/j.carbon.2005.04.008)
- [34]. X.L. Zhou, Q. Tan, G.X. Yu, L.F. Chen, J.A. Wang, O. Novaro, *Kinet. Catal.* 50 (2009) 543–549. DOI: [10.1134/S0023158409040119](https://doi.org/10.1134/S0023158409040119)
- [35]. K.G. Haw, W.A.W.A. Bakar, R. Ali, J.F. Chong, A.A.A. Kadir, *Fuel Proc. Tech.* 91 (2010) 1105–1112. DOI: [10.1016/j.fuproc.2010.03.021](https://doi.org/10.1016/j.fuproc.2010.03.021)
- [36]. J. Xiao, L. Wu, Y. Wu, B. Liu, L. Dai, Z. Li, Q. Xia, H. Xi, *Appl. Energy* 113 (2014) 78–85. DOI: [10.1016/j.apenergy.2013.06.047](https://doi.org/10.1016/j.apenergy.2013.06.047)
- [37]. M.T. Timko, J.A. Wang, J. Burgess, P. Kracke, L. Gonzalez, C. Jaye, D.A. Fischer, *Fuel* 163 (2016) 223–231. DOI: [10.1016/j.fuel.2015.09.075](https://doi.org/10.1016/j.fuel.2015.09.075)
- [38]. W. Zhang, H. Zhang, J. Xiao, Z. Zhao, M. Yu, Z. Li, *Green Chem.* 16 (2014) 211–220. DOI: [10.1039/C3GC41106K](https://doi.org/10.1039/C3GC41106K)
- [39]. Q. Gu, G. Wen, Y. Ding, K.H. Wu, C. Chen, D. Su, *Green Chem.* 19 (2017) 1175–1181. DOI: [10.1039/C6GC02894B](https://doi.org/10.1039/C6GC02894B)
- [40]. S.C. Tsang, Y.K. Chen, P.J.F. Harris, M.L.H. Green, *Nature* 372 (1994) 159–162. DOI: [10.1038/372159a0](https://doi.org/10.1038/372159a0)
- [41]. F. Tuinstra, J.L. Koenig, *J. Chem. Phys.* 53 (1970) 1126–1130. DOI: [10.1063/1.1674108](https://doi.org/10.1063/1.1674108)
- [42]. S. Costa, E. Borowiak-Palen, M. Kruszyńska,

- A. Bachmatiuk, R.J. Kalenczuk, *Mater. Sci.-Poland* 26 (2008) 433–441.
- [43]. O.S. Timofeev, N.G. Chechenin. Proceedings of the XII Interuniversity scientific school of young specialists “Concentrated energy flows in space technology, electronics, ecology and medicine”. Moscow 21-22 November 2011, p. 118–123 (in Russian).
- [44]. G. Socrates. *Infrared and Raman Characteristic Group Frequencies. Tables and Charts*. Third Edition. John Wiley & Sons Ltd. 2001.
- [45]. Z.R. Ismagilov, A.E. Shalagina, O.Yu. Podyacheva, A.V. Ischenko, L.S. Kibis, A.I. Boronin, Y.A. Chesalov, D.I. Kochubey, A.I. Romanenko, O.B. Anikeeva, T.I. Buryakov, E.N. Tkachev, *Carbon* 47 (2009) 1922–1929. DOI: [10.1016/j.carbon.2009.02.034](https://doi.org/10.1016/j.carbon.2009.02.034)
- [46]. T.G. Ros, A.J. van Dillen, J.W. Geus, D.C. Koningsberger, *ChemPhysChem* 3 (2002) 209–214. DOI: [10.1002/1439-7641\(20020215\)3:2<209::AID-CPHC209>3.0.CO;2-S](https://doi.org/10.1002/1439-7641(20020215)3:2<209::AID-CPHC209>3.0.CO;2-S)
- [47]. L. Stobinski, B. Lesiak, L. Kövér, J. Tóth, S. Biniak, G. Trykowski, J. Judek, *J. Alloys Compd.* 501 (2010) 77–84. DOI: [10.1016/j.jallcom.2010.04.032](https://doi.org/10.1016/j.jallcom.2010.04.032)
- [48]. S. Kundu, Y. Wang, W. Xia, M. Muhler, *J. Phys. Chem. C* 112 (2008) 16869–16878. DOI: [10.1021/jp804413a](https://doi.org/10.1021/jp804413a)
- [49]. L.C.A. Oliveira, C.N. Silva, M.I. Yoshida, R.M. Lago, *Carbon* 42 (2004) 2279–2284. DOI: [10.1016/j.carbon.2004.05.003](https://doi.org/10.1016/j.carbon.2004.05.003)
- [50]. Z. Zhou, E.K. Orcutt, H.C. Anderson, K.J. Stowers, *Carbon* 152 (2019) 924–931. DOI: [10.1016/j.carbon.2019.06.076](https://doi.org/10.1016/j.carbon.2019.06.076)
- [51]. J.L. Figueiredo, M.F.R. Pereira, M.M.A. Freitas, J.J.M. Orfao, *Carbon* 37 (1999) 1379–1389. DOI: [10.1016/S0008-6223\(98\)00333-9](https://doi.org/10.1016/S0008-6223(98)00333-9)
- [52]. I. Graca, L.V. Gonzalez, M.C. Bacariza, A. Fernandes, C. Henriques, J.M. Lopes, M.F. Ribeiro, *Appl. Catal. B* 147 (2014) 101–110. DOI: [10.1016/j.apcatb.2013.08.010](https://doi.org/10.1016/j.apcatb.2013.08.010)
- [53]. H. Zhao, C. Xu, T. Wang, *Sustainable Chemistry and Pharmacy* 13 (2019) 100150. DOI: [10.1016/j.scp.2019.100150](https://doi.org/10.1016/j.scp.2019.100150)